POLITECNICO DI TORINO
Repository ISTITUZIONALE

Tape winding angle influence on subsea cable sheathing fatigue performance

(Article begins on next page)

20 April 2024
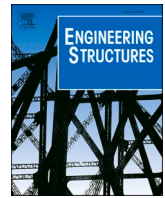
Tape winding angle influence on subsea cable sheathing fatigue performance

Luigi Mario Viespoli [a,d,*], Luigi Panza [a,b], Audun Johanson [c], Antonio Alvaro [a,b,c,d], Aurelio Somà [b], Filippo Berto [a]

[a] Department of Mechanical and Industrial Engineering, Norwegian University of Science and Technology (NTNU), Richard Birkelands vei 2B, 2034 Trondheim, Norway
[b] Dipartimento di Ingegneria Meccanica e Aerospaziale, Politecnico di Torino, Italy
[c] Nexans Norway, Innspurten 9, 0663 Oslo, Norway
[d] Sintef Industry, Richard Birkelands vei 2B, 7031 Trondheim, Norway

ABSTRACT

A fundamental component of subsea power cables is the thin galvanized steel tape winded around the dielectric and sheathing layer in order to prevent permanent thermal cycling induced deformation. The pressure state induced by the resistance offered by such tapes against radial reformation reduces the triaxiality ratio of the stress state of the lead sheathing layer. It is known that a reduced triaxiality has a beneficial effect on ductility and fatigue life of metals. In the present work a series of finite element simulations are performed in presence of galvanized steel tapes at three different winding angles and without such reinforcement at all, obtaining a qualitative indication of its effect on the stress state induced in the sheathing layer. Loading conditions as internal pressure related to thermal dielectric expansion and cable bending are modelled. The numerical qualitative results are discussed in connection to a series of full-scale fatigue tests performed on subsea power cables with and without the support of steel tapes.

1. Introduction

The fatigue behaviour of subsea high voltage cable sheathing, produced by extrusion of lead alloys, is affected by the design of the cable and by time dependent deformation and damage mechanisms. The operational temperature for the sheathing layer lies around room temperature or slightly above. The low melting point characterizing the lead alloys industrially adopted for this component is generally inferior to 600 K, barely twice as much as the operational temperature.

Being the use of lead alloys as extrusion material for cable sheathing a specialized topic, often laying in the boundaries of the industrial secrecy and a relatively old technology, the amount of available literature regarding the subject is limited and most of it was produced several decades ago. An investigation on creep behaviour of cable sheathing lead alloys was published by the University of Illinois evidencing, at three different temperatures, time dependent deformation even for very low stresses and a marked effect of pulling speed on tensile resistance [1] and the effect of alloying elements, thermal treatments and cyclic loading [2]. The creep behaviour of polycrystalline lead and the

influence of mean grain diameter was investigated by Feltham [3], while the fatigue properties of some alloys of interest for the cable industry was published by Havard [4]. Testing on the topic of fatigue life of lead alloys for subsea power cables was performed by Società Cavi Pirelli [5] while Sahota and Riddington investigated the response to compressive loads for various lead alloys [6].

In the recent years, the industrial will to obtain a deeper understanding of the materials used in production and optimize alloys and design for economic and environmental purposes has led to a new series of investigations with modern techniques. The studies performed regarded the tensile behaviour and microstructure [7], influence of production defects on fatigue life [8,9], steady state creep [10] and fatigue results of full-scale testing [11].

Research papers focused on the FEM analysis of subsea power cables are not numerous, especially for what regards the mechanical aspect. Some interesting contributions are the works of Huang et al. [12,13].

The present work utilizes the material properties obtained in the tensile testing and the creep model calibrated based on the test results from [7] to perform a qualitative numerical investigation on the

Table 1

MI HVDC cable cross section component list and dimensions. Parts A to H correspond to the assembly components in the FE model.

Part	Components	Description	Material	t (mm)	Rint (mm)	Rext (mm)
A	1	Conductor	Copper			23.15
	2	Conductor screen	Carbon black paper tapes	0.4	23.15	23.55
B	3	Insulation	Impregnated paper tapes	20.15	23.55	43.7
	4	Insulation screen	Carbon black paper and metallized paper tapes			
	5	Serving	Copper woven fabric tape			44.6
C	6	Lead Sheath	E-Alloy	3.3	44.6	47.9
D	7	PE Sheath	PE	3.3	47.9	51.2
	8	Bedding	Semi conductive nylon tape			
E	9	Reinforcement	Galvanized Steel	0.8	51.2	52
	10	Bedding	Semi conductive nylon tape			
F	11	Armor wires	Galvanized Steel GR34	3	52	55
	12	Bedding	Plastic coated nylon tape			
G	13	Armor wires	Galvanized Steel GR34	3	55	58
	14	Bedding	Plastic coated polyester tape			
H	15	Outer Sheath	HDPE	6	58	64

influence of the compressive stresses introduced in the sheathing layer by the winding of tensioned steel tapes. The full-scale fatigue results [11] are discussed focusing on the influence of stress triaxiality on the fatigue life of metallic alloys.

2. Short notes on triaxiality

Experimental evidence in creep-fatigue models and multi-axial fatigue conditions shows that a triaxial stress state influences the fatigue life of a ductile metal and such influence is accounted for in some failure models. For example, the Strain Range Partitioning (SRP) method applied under multi-axial conditions [14] uses the concept of Multiaxiality Factor (MF) for the assessment of the creep-fatigue damage. The same MF is used in the total equivalent strain range method modified by multiaxiality factor [15] for the evaluation of the fatigue life. In both theories, MF is defined as a function of the Triaxiality Factor (TF). TF is defined as the ratio between the mean stress σ_m, representative of the hydrostatic state of material, and the Von Mises equivalent stress σ_{eq}, representative of the deviatoric state of material.

$$TF = \frac{\sigma_m}{\sigma_{eq}} \tag{1}$$

The Multiaxiality Factor is so defined [14]:

$$MF = TF \, for \, TF \geq 1$$

$$MF = \frac{1}{(2 - TF)} for \, TF \leq 1 \tag{2}$$

For example, the strain-life equation of total equivalent strain range method modified by Multiaxiality Factor is: [15]

$$\Delta\varepsilon_{eq} = MF^{-b/c}B\big(N_f\big)^b + \frac{C}{MF}\big(N_f\big)^c \tag{3}$$

where B, C, b and c are material constants. It's possible to observe that when MF > 1 the fatigue curve downshifts towards lower strain ranges, while when MF < 1 the fatigue curve shifts upwards. The same reasoning is valid for what concerns the SRP method under multiaxial conditions, where MF contributes to move the fatigue line influencing the creep damage by modifying the creep ductility.

3. Subsea cable fatigue scenarios and full-scale testing

Lead testing and fatigue performance appear to be particularly sensitive to loading mode and interaction with other components. As such it is necessary to validate the fatigue life by component or full-scale testing.

Fatigue and creep damage arise from multiple sources during the cable operational life. This includes bending due to wave motion during

offshore installation or recovery operations, High frequency bending in the case of free spans on the seabed, or slow frequency radial displacement under thermal fluctuation. We focus on testing by reversed bending to simulate the former scenarios. The lead sheathed power phase is axially load controlled while displaced in the parallel direction by shapers with fixed radius. A given shaper radius will induce a corresponding $\Delta\varepsilon$ in the lead sheathing which is related to the lead sheath's diameter. Although the actual strain was not measured, the contact between the shaper and test object was visually controlled. All tests were conducted at room temperature. Power phases with and without transversal armour were both tested. The former corresponds to a typical Mass Impregnated High Voltage Direct Current cable (MI HVDC), while the latter corresponds to a Cross-linked Polyethylene (XLPE) power phases [11].

4. Cable modelling

4.1. Schematization of the cable

In order to better understand the results obtained in the full-scale testing campaign a series of numerical simulations were performed. A Nexans 525 kV Mass-impregnated (MI) HVDC subsea cable was chosen as model geometry for the simulation. The fifteen components of the cable are listed in table 1 and the multi-component finite element model was created by assembling a series of eight parts, listed in Table 1 as A to H. That is, the layers 2, 4, 5, 8, 10, 12 and 14 in Table 1 have been suppressed and their volume merged with the volume of the main component they are winded around. This simplification was performed in the hypothesis that, given the small thickness of these components compared to the thickness of the other layers, these layers do not significantly contribute to the radial stiffness of the cable, which is determinant for the compressive stress induced in the lead sheathing. The modification of the structure from the real component 1–15 into the FEM parts A-H according to the hypothesis described significantly reduces the computational cost of the model. Conductor, reinforcements, insulants and armours were modelled as continue bodies. The FE model corresponds to a cable length of 2 m, that is over the pitch length of the longitudinal armour.

4.2. Material properties

The material properties are chosen to model the assembly in a meaningful way, with the main focus on the rate dependent behaviour of the lead sheathing. Severe simplifications had to be made on some of the other component. However, since the scope of the work is to gain a better understanding of the qualitative influence of the reinforcement tapes and their configurations on the cable fatigue behaviour and these simplifications allow to perform the modelling efficiently with respect to

Table 2
Synthesis of the material properties implemented.

COMPONENT	INPUT DATA
Conductor	Type of material: Copper
	Elastic behaviour: E = 120000 MPa, ν = 0.34
Insulation system	Type of material: Kraft paper, oil, copper tapes
	Elastic behaviour: E = 19340 MPa, ν = 0.44
Lead sheath	Type of material: E-Alloy
	Elastic behaviour: E = 12000 MPa, ν = 0.431
	Plastic behaviour: see relative table
	Creep behaviour: A = 5.278e-10, m = -0.47, n = 5.22
PE sheath	Type of material: PE
	Elastic behaviour: E = 600 MPa, ν = 0.46
	Plastic behaviour: see relative table
Reinforcement	Type of material: galvanized steel tapes
	Winding angle: 70 degrees from the cable axis
	Orthotropic elastic behaviour: see relative table
Armour 1	Type of material: galvanized steel wires
	Winding angle: 12.7 degrees from the cable axis
	Orthotropic elastic behaviour: see relative table
Armour 2	Geometry, type of material: galvanized steel wires
	Winding angle: −10.5 degrees from the cable axis
	Orthotropic elastic behaviour: see relative table
Outer sheath	Type of material: HDPE
	Elastic behaviour: E = 780 MPa, ν = 0.46
	Plastic behaviour: see relative table

Table 3
Elastic-plastic properties of: C component (a), D component (b), H component (c).

a) E (MPa)	12,000		b) E (MPa)	600		c) E (MPa)	780	
ν	0.431		ν	0.46		ν	0.46	
ε_pl	σ (MPa)		ε_pl	σ (MPa)		ε_pl	σ (MPa)	
0	7.4		0	2		0	10	
0.000006	7.9		0.015	3		0.2	10	
0.00013	8.45		0.023	4		0.5	10	
0.00044	10.5		0.04	6		0.8	10	
0.0008	11.6		0.09	7.5		1	10	
0.00129	12.26		0.19	9		1.5	10	
0.0024	13.15		0.29	9.5		1.7	10.5	
0.0052	14.3		0.39	10		2	11.75	
0.0088	15.25		0.49	10.5		3	14	
0.0248	17.3		0.59	11		4	17	
			0.69	11.5		5	20	
			0.79	12.5				
			0.89	13				
			0.99	13.5				

Table 4
Elastic table for the armoring components (E, F, G). They are defined in their own reference system.

Orthotropic elastic behavior with transversely isotropic elasticity		
E1	2000	MPa
E2	2000	MPa
E3	200,000	MPa
Nu12	0,3	
Nu13	0,003	
Nu23	0,003	
G12	769	MPa
G13	770	MPa
G23	770	MPa

On the other hand, modelling the individual strands helically wound is highly demanding from a computational point of view and not necessary for the scope of this analysis, which focused on the lead sheathing. Therefore, the coupling of the torsional and of the flexural behaviour in the two longitudinal planes due to the helical winding of the strands is neglected.

The insulation system (B) is a challenging component to model in a practical and realistic way since it requires several assumptions to be approximated by a simple assembly component. In mass impregnated cables, Kraft paper impregnated by high viscosity oil is used as main electrical insulation layer. Typically, the range of temperature experienced by the cable during the service is between the seabed temperature for the outer layer and 50 to 80 degreesC for the insulation [13], low enough to consider the oil always with high viscosity. The choice of the authors was to approximate it by a simple isotropic elastic component. Although the authors are aware that this constitutes a heavy approximation, the scope of the study is to investigate the influence of steel tapes winding angle on the lead sheathing layer. The insulation is then simply considered as a solid between the conductor and the external layers [13]. It is necessary to calculate an equivalent elastic modulus the B part from the constitutive components, the Kraft paper, the oil giving compression stiffness and the outer copper woven fabric tape. These components are treated as parallel springs because subjected to the same curvature Γ caused by the bending load M_f.

$$k_{f,i} = E_i I_{f,i} \tag{4}$$

$$M_f = \Gamma k_{f,eq} = \Gamma \sum \left(E_i I_{f,i} \right) = \Gamma E_{eq} I_{f,eq} \tag{5}$$

$$E_{eq} = \frac{\sum \left(E_i I_{f,i} \right)}{I_{f,eq}} \tag{6}$$

where $k_{f,i}, E_i, I_{f,i}$ are respectively the bending stiffness, the elastic modulus and the bending inertia of the single parts and $E_{eq}, I_{f,eq}$ are respectively the equivalent elastic modulus and the equivalent bending inertia of the system. The equivalent Poisson's ratio ν_{eq} was computed as a volume weighted average of the ratios of the relevant components.

$$\nu_{eq} = \frac{\sum \left(\nu_i V_i \right)}{V_{eq}} \tag{7}$$

where ν_i, V_i, V_{eq} are respectively the Poisson's coefficients, the volumes and equivalent volume of the parts included in computation.

The lead sheathing (C) was modelled using the strain hardening power law creep behaviour available in Abaqus. The properties were calibrated by tensile testing at different strain rates reported by Viespoli et al. [7]. The material is a lead alloy commercially known as E-Alloy, with the following chemical composition: Pb 99,3 wt%, Sb 0,2 wt%, Sn 0,5 wt%. For the sake of completeness, the formulation of the material model is reported in Eq. (8):

$$\dot{\varepsilon}_{eq,cr} = \left\{ A\sigma_{eq,d}^{n} \left[(m+1)\varepsilon_{eq,cr} \right]^{m} \right\}^{\frac{1}{m+1}} \tag{8}$$

where A, m, n are material constants and $\sigma_{eq,d}$ and $\varepsilon_{eq,cr}$ are the equivalent Von Mises stress and the equivalent creep strain, respectively.

The polyethylene layer (D) is modelled as a simple elastic–plastic material. The material properties implemented are provided by Nexans Norway and all effects of strain rate on the polymer's response are neglected.

The reinforcement (E) is constituted by galvanized steel tape winded over the component D and its influence is the fundamental object of study in this work. For optimizing the pre-processing and the computational time, the tape was modelled as a continuous body with orthotropic elastic properties, having the maximum stiffness, corresponding to the stiffness of steel, along the winding direction and a stiffness several orders of magnitude lower in the other directions. The
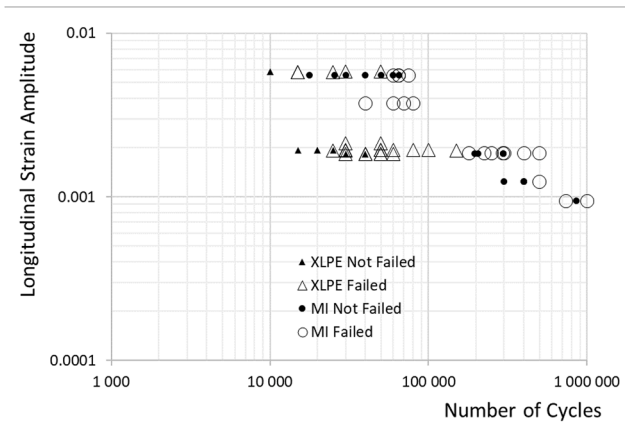
the aforementioned objective. The description of the material properties for each part included in the model is presented in this paragraph and the mechanical properties are the listed in Tables 2–4.

The conductor (A) is made of very commercially pure copper and its mechanical behaviour was modelled as isotropic linear elastic material so that only two parameters are necessary: the elastic modulus and the Poisson's coefficient. These values can be easily found in the literature.

Fig. 1. Full scale fatigue testing results. The MI cable showed considerably better fatigue performance [11].

orthotropic elastic behaviour with transversely isotropic elasticity was chosen from the Abaqus library and, for its implementation, a cylindrical reference system was created for each orthotropic component and rotated accordingly to the winding direction.

Two layers of armour are introduced in these cables with the main purpose of providing axial strength for the cable to sustain its own weight during installation. The armour is made of galvanized steel wires with a thickness of 3 mm and was modelled as an orthotropic material in the same way adopted for the steel tapes. The maximum resistance direction corresponds to the wire axis, which is at an angle from the cable's longitudinal direction of $12.7°$ for the inner armour (F) and $-10.5°$ for the outer armour (G).

The high-density polyethylene outer sheathing (H) is model, as for the component D, as an elastic–plastic isotropic continuum, neglecting the rate dependent effects, according to the data provided by the producer.

4.3. Meshing

Each component of the cable assembly was discretized using three-dimensional quadratic elements. After an initial phase of mesh size optimization, the following element dimensions were used for the analysis: a characteristic element size of 20 mm was used in the longitudinal direction, while 24 elements around the circumference in the tangential direction were used for components A and B, 48 elements were used for components C to H in order to obtain a finer mesh for the thinner components. With respect to the radial discretization, the A and B parts have 5 elements through the thickness, while all the other components have 2 elements through the thickness. These values have

been verified to provide reliable results with respect to the required accuracy. A total of 78,000 elements and 412,389 nodes was generated, see Fig. 2.(See Fig. 3)

4.4. Boundary conditions

Surface Interactions: Surface-based tie constraints were implemented as interactions between the various parts of the model. This kind of interaction constraints the connected surfaces so to have the same displacement: separation and sliding between surfaces are not allowed. Such hypothesis is valid for most operational conditions when the static slipping resistance of the bedding layers is not exceeded, which is relevant for most operational conditions. A manual attribution of the master and slave surface makes for a more efficient model solution. The nodes on the slave surface must have the same motion of the master surface nodes and the master surface should be stiffer than the slave master, thus, a stiffer material and coarser mesh are conditions for the choice of the master surface. Two tie formulations are available in Abaqus: the surface-to-surface formulation and the node-to-surface formulation. The surface-to-surface formulation generally avoids stress noise at tied interfaces. Moreover, with a surface-to-surface approach,
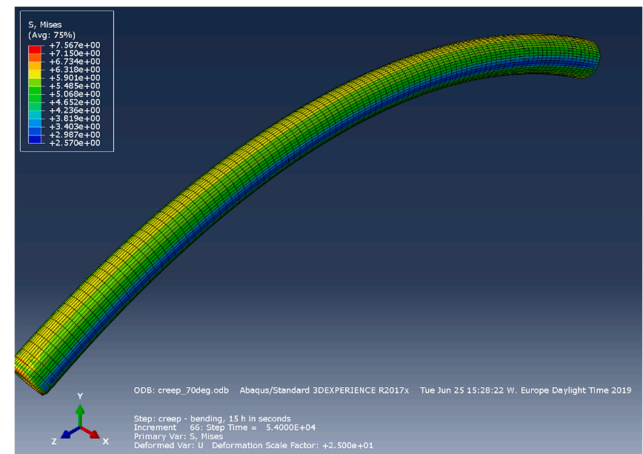

Fig. 3. Deformed lead sheathing layer.

Table 5
Master/slave surface attribution.

Interaction	AB	BC	CD	DE	EF	FG	GH
Master	A_ext	B_ext	C_ext	E_int	F_int	G_int	G_ext
Slave	B_int	C_int	D_int	D_ext	E_ext	F_Ext	H_int

A: conductor
B: insulation
C: lead sheath
D: PE sheath
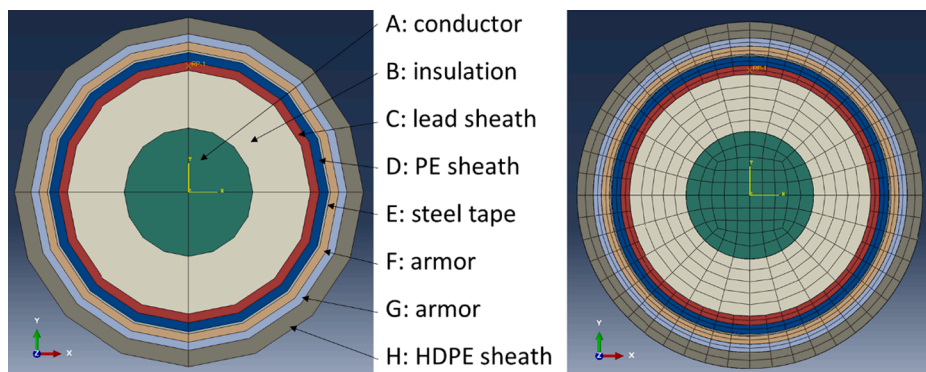E: steel tape
F: armor
G: armor
H: HDPE sheath

Fig. 2. Abaqus assembly of parts A to H (Left). Cross section of FEM discretization with reference point RP-1 of extraction of the stress output for the lead sheathing (Right).
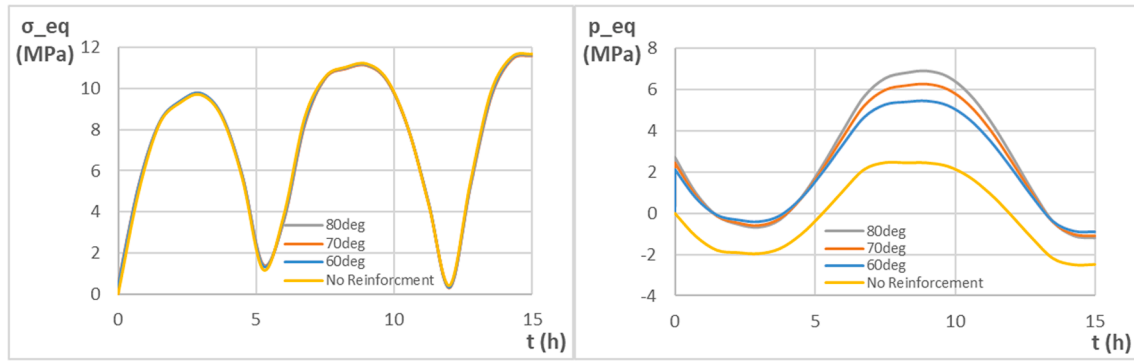
Fig. 4. Non time-dependent modelling of test like situation.

there is less sensitivity related to the choice of master and slave surfaces. Based on these considerations, a surface-to-surface approach was selected and the attribution of the master/slave surfaces is summarized in table 5.

External Constraints: The model cable was constrained at the two extremes. Depending on the simulated scenario these sections were either one fully constrained and the other allowed to translate longitudinally or the longitudinal translation and rotation in a longitudinal cutting plane were allowed. Further details are provided in the load-cases paragraph.

Load cases: In the present study a series of different load cases and cable designs were implemented to evaluate the influence of the different parameters on the stress state of the lead sheathing. The load cases implemented are described below:

- *Pre-tensioning of the tape*

The application of the steel tapes on the underlying lead sheath with a certain pre-tensioning was simulated as a cooling of the E component. A typical thermal expansion coefficient of 3,5e-5 (1/K) for the steel was assumed, and a negative thermal excursion was simulated in order to obtain a pre-stress of about 200 MPa along the winding direction of the tape.

- *Sea water pressure*

A representative sea depth of 100 m, corresponding to and external pressure of 1 MPa, was chosen. This value causes a slight increase in the compressive state of the underlying layers, but no deviatoric stress.

- *Thermal expansion of the insulation system*

The insulation layer's thermal expansion due to Joule heating was modelled considering assumptions similar to previous works on the topic of subsea power cables [13]. The initial temperature of submarine ambient can be assumed to be of about 4 degreesC while at regime conditions, the temperature at the interface between insulation system and lead sheath is around 50 degreesC [13]. Only the heating of the B component was modelled because the thermal expansion coefficient of oil is considerably higher than that of the other components [13]. A typical value for the thermal expansion coefficient of the oil is 6.3E-4 1/K [16]. The oil occupies only a certain fraction of the insulation system. This fraction depends on the impregnation level and is defined as the ratio between the oil volume and the total insulation volume. This value is useful in order to compute a reasonable approximation of the thermal expansion coefficient of the assembly. Typical values are comprised by 0.3 to 0.7, but often is used 0.4 [16]. This value is multiplied by the thermal expansion coefficient of the oil to approximate the thermal expansion coefficient of the B component. The oil impregnated paper insulation is affected by the presence of cavities. While the layer heats

up, these cavities are filled by the oil until a threshold temperature, referred to as the cavity free temperature, is reached. Above this temperature the insulation starts expanding and pressure builds up as a consequence of the presence of the layers above. A typical value of cavity free temperature is about 30 degreesC [16]. Therefore, a reasonable thermal excursion to attribute for the thermal load modelling is about 20 degreesC.

- *Cyclic bending*

Pure bending condition was assumed in order to analyse the bending behaviour of the cable in the full-scale testing and due to the wave motion in the hypothesis of use as dynamic cable. The two extremes of the cable were rigidly rotated over time, keeping the cable at a constant curvature over its length. The amplitude of the rotations was defined as a sinusoidal wave with zero mean for a 12 h period. Since the simulations were run both with and without the presence of creep deformation, this long period was chosen to be able to discern the sheathing's behaviour when subjected to a high strain rate (corresponding to absence of creep deformation) and to a very low one (creep deformation included and 12 h period). The real response of the material to both the full-scale testing and to tidal motion will be in the middle of these extremes. A simulation time of 15 h was used, corresponding to 1.25 periods, starting from the undeformed position. The strain amplitude imposed at the level of the C component, of 0.001, was selected in order to be of the same order of magnitude of that of the full-scale testing. The maximum curvature Γ to impose to the cable to reach this value of deformation was computed following the theory of beams:

$$\Gamma = \frac{\varepsilon_{long}}{r_{ext}} = 1,25 \ ^{\circ}/m \tag{9}$$

where ε_{long} and r_{ext} are the maximum longitudinal total strains of the lead sheath.

4.5. FEM cable designs

Three different winding angles, measured from the longitudinal direction, of the steel tapes were considered in order to verify the effect of this parameter on the stress state of the lead sheath. The winding angle was in practice modelled as a rotation of the coordinate system in which the orthotropic layer's properties are defined. A fourth design, that is a cable in which the tape is replaced by a PE sheathing, was also modelled. In summary, the four models are characterized as follows: 60°, 70°, 80° for the winding angle of the reinforcement and absence of the steel tapes.

5. Numerical results

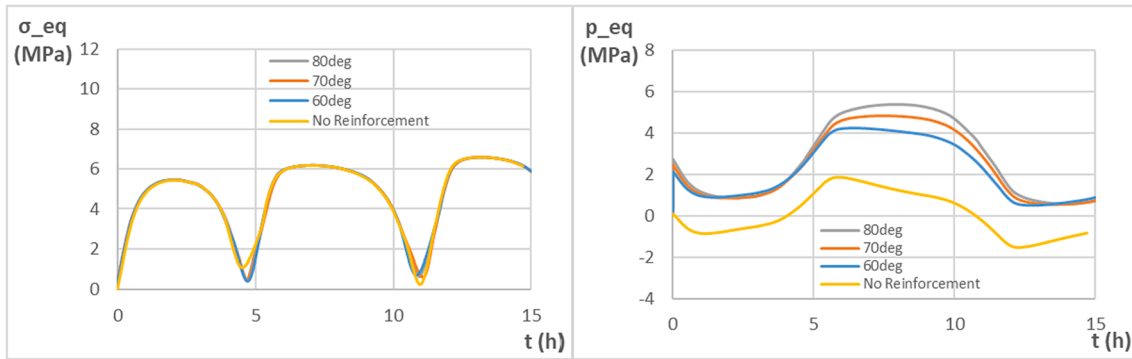The numerical modelling previously described was used to simulate two different scenarios:

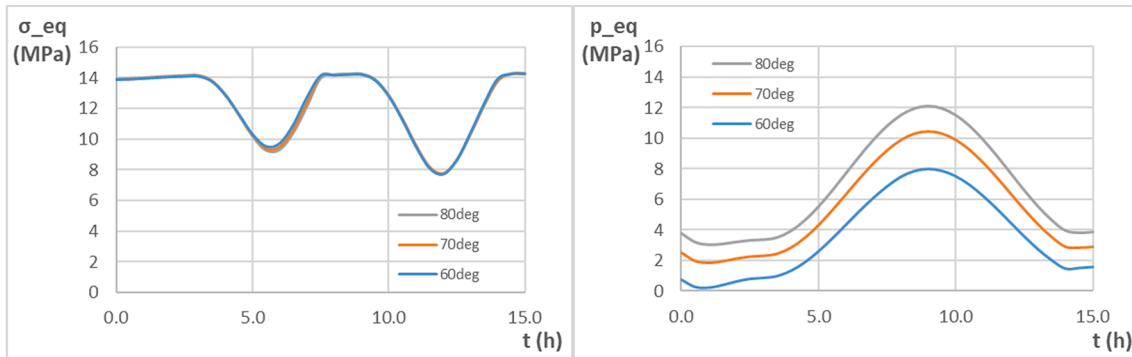**Fig. 5.** Time-dependent modelling of test like situation.

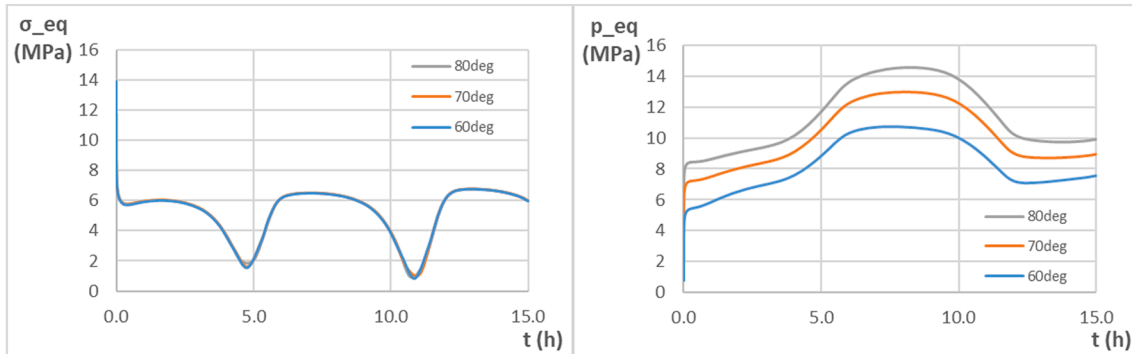**Fig. 6.** Non time-dependent modelling of dynamic cable operation like situation.

Fig. 7. Time-dependent modelling of dynamic cable operation like situation.

- Pre-tensioning of the steel tapes and subsequent cyclic bending, condition equivalent to the testing procedure, in which the cable is not subjected to the internal heating and consequent expansion.
- Sea water pressure, thermal expansion of the insulation system and subsequent cyclic bending in order to evaluate the response of the

Table 6
Average triaxiality factor in the lead sheathing modelling a full-scale testing like situation.

Full scale testing modelling	STATIONARY SIMULATION	VISCOUS SIMULATION
Winding angle of tape	**Cyclic mean TF (3–15) h**	**Cyclic mean TF (3–15) h**
Absence of tape	−0.01	−0.03
60 degrees	−0.76	−0.74
70 degrees	−0.90	−0.81
80 degrees	−1.02	−1.10

lead sheathing also with the internal pressure due to the operational conditions in the hypothesis of use in a dynamic application.

These simulations where run modelling the lead sheathing both with the strain hardening power law creep model described in the previous section and by attributing to this layer only the elastic plastic properties without any time dependent behavioural components. This is done to investigate the influence of the creep behaviour on the relaxation of deviatoric stress, but not of the hydrostatic stress, thus increasing the negative magnitude of the stress triaxiality factor. Consequently, the results of a total of 14 simulations are reported in Figs. 4–7.

For every simulation, as shown in the following representative figures, there isn't a significative gradient in the stress–strain field along the longitudinal direction, thus, the results were extracted in the lead sheathing's mid-thickness point of the middle section of the cable, see Fig. 2. From the two most significative diagrams of both kinds of simulation, can arise the following considerations:

Table 7

Average triaxiality factor in the lead sheathing modelling a dynamic cable in an operation like situation.

Dynamic cable modelling	STATIONARY SIMULATION	VISCOUS SIMULATION
Winding angle of tape	**Cyclic mean TF (3–15) h**	**Cyclic mean TF (3–15) h**
60 degrees	−0.37	−2.11
70 degrees	−0.54	−2.52
80 degrees	−0.66	−2.89

- The winding angle of the steel tapes does not influence the Von Mises equivalent stress.
- The winding angle of the steel tapes affects the equivalent pressure. An increase of the winding angle is followed by an increase of the equivalent pressure.
- Considering the average value of the stress triaxiality factor on a cycle (calculated in the span 3–15 h), it's possible to compute the cyclic average TF for the different cases modelled. The results are shown in the following tables and figures.

The results in table 6 summarize the average triaxiality factor over a bending cycle, that is modelling the full-scale testing conditions. In absence of steel tape, the triaxiality factor is virtually zero, while it becomes a negative value comprised between −0.74 and −1.10 considering the presence of the steel tape and its winding angle from the longitudinal direction. Analysing these results in light of the theory on the effect of the triaxiality factor on fatigue life it is predictable that the presence of the tapes, with their pre-tensioning, introduces a beneficial compressive stress which will improve the fatigue life. This is in agreement with the experimental results in Fig. 1, where is clearly seen how lead sheathing of the MI HVDC cables, which have the steel tapes in their design, has better fatigue performance than that of the XLPE ones, in which the tapes are absent.(See Table 7)

6. Conclusions

In this work the results of a qualitative numerical investigation on the influence of cable's design parameters on the fatigue performance of the lead sheathing layer of subsea high voltage cables is presented. Some cables have galvanized steel tapes winded over the lead sheathing layer to limit tangential deformations due to thermal expansion. Full scale fatigue testing results in presence and absence of such tapes are available in the literature and show improved fatigue performances for cable designs which include the reinforcement tapes. It is known that a prevalence of hydrostatic compression, quantified with a negative triaxiality factor, has a positive effect on the fatigue life of metals. In this work the cable was modelled with certain designs and boundary conditions: without tapes and with tapes winded at different angles in a full-scale test-like situation and in a dynamic-operation-like situation, both including and excluding the effect of creep deformation. The stress state detected in the lead sheathing indicates an increase of hydrostatic compression induced by the steel tapes. This is in good agreement with the experimental results, providing an explanation for the better fatigue performance of the lead sheathing layer of cable designs including the steel tapes as a consequence of the modification of the stress triaxiality. This effect is enhanced by the presence of creep deformation, which contributes to reduce the deviatoric stress in the sheathing for low strain rate deformations.

Declaration of Competing Interest

The authors declared that there is no conflict of interest.

Acknowledgements

Appendix:. Lead sheathing contour plots

Fig. 8 contains a series of contour plots of the hydrostatic pressure and Von Mises stress of the lead sheathing under different configurations and loading conditions, after bending deformation. The conditions of each plot are summarized in Table 8.
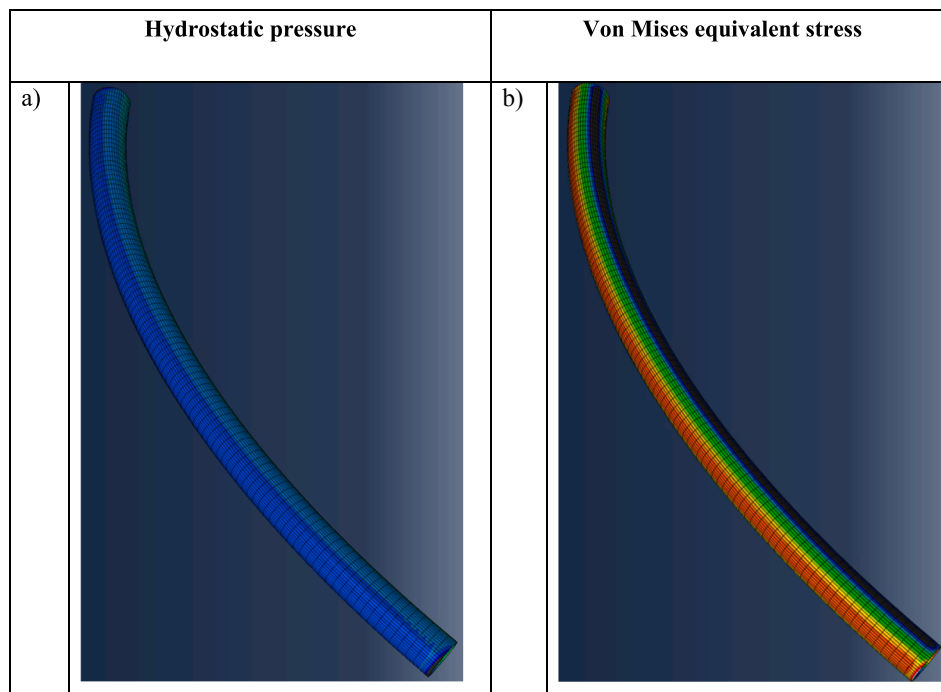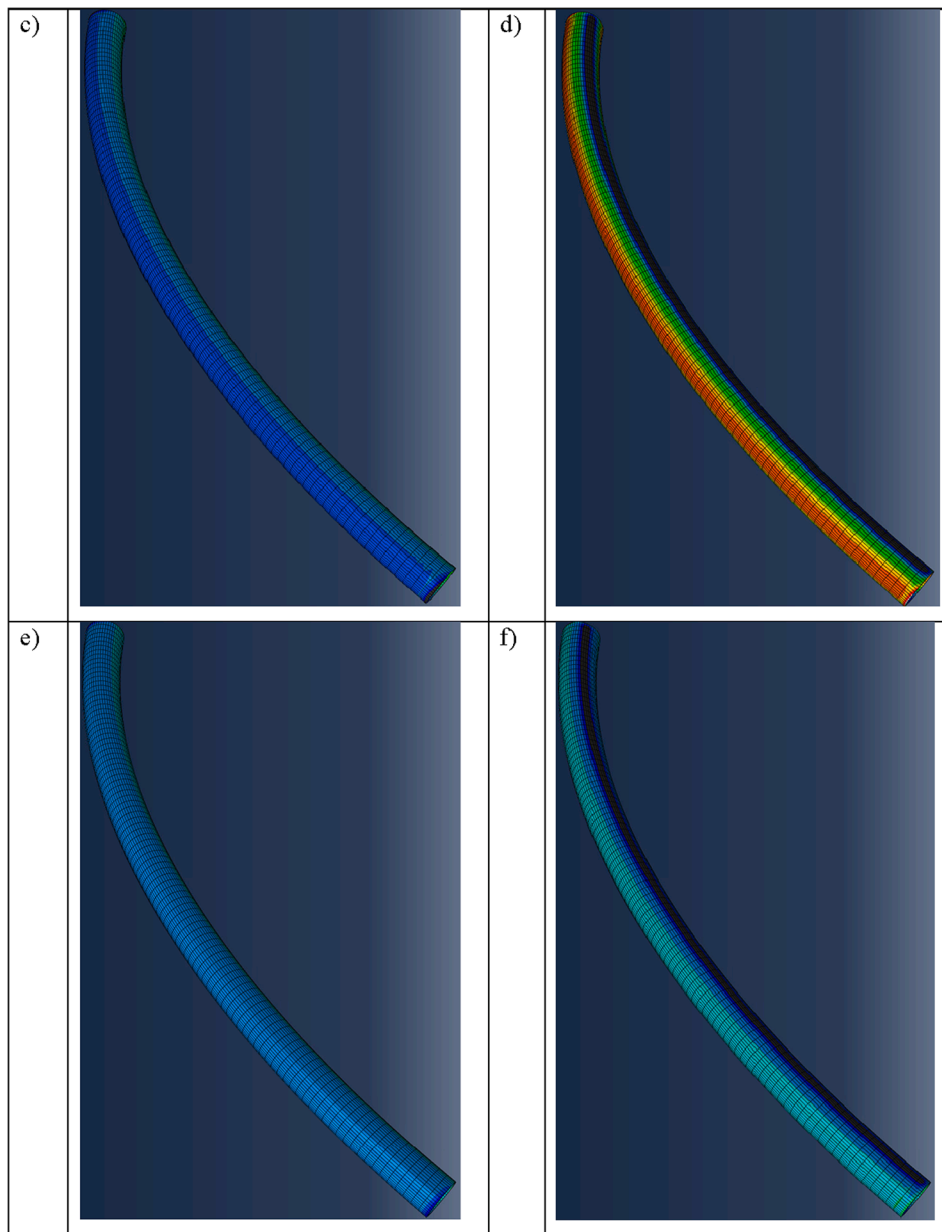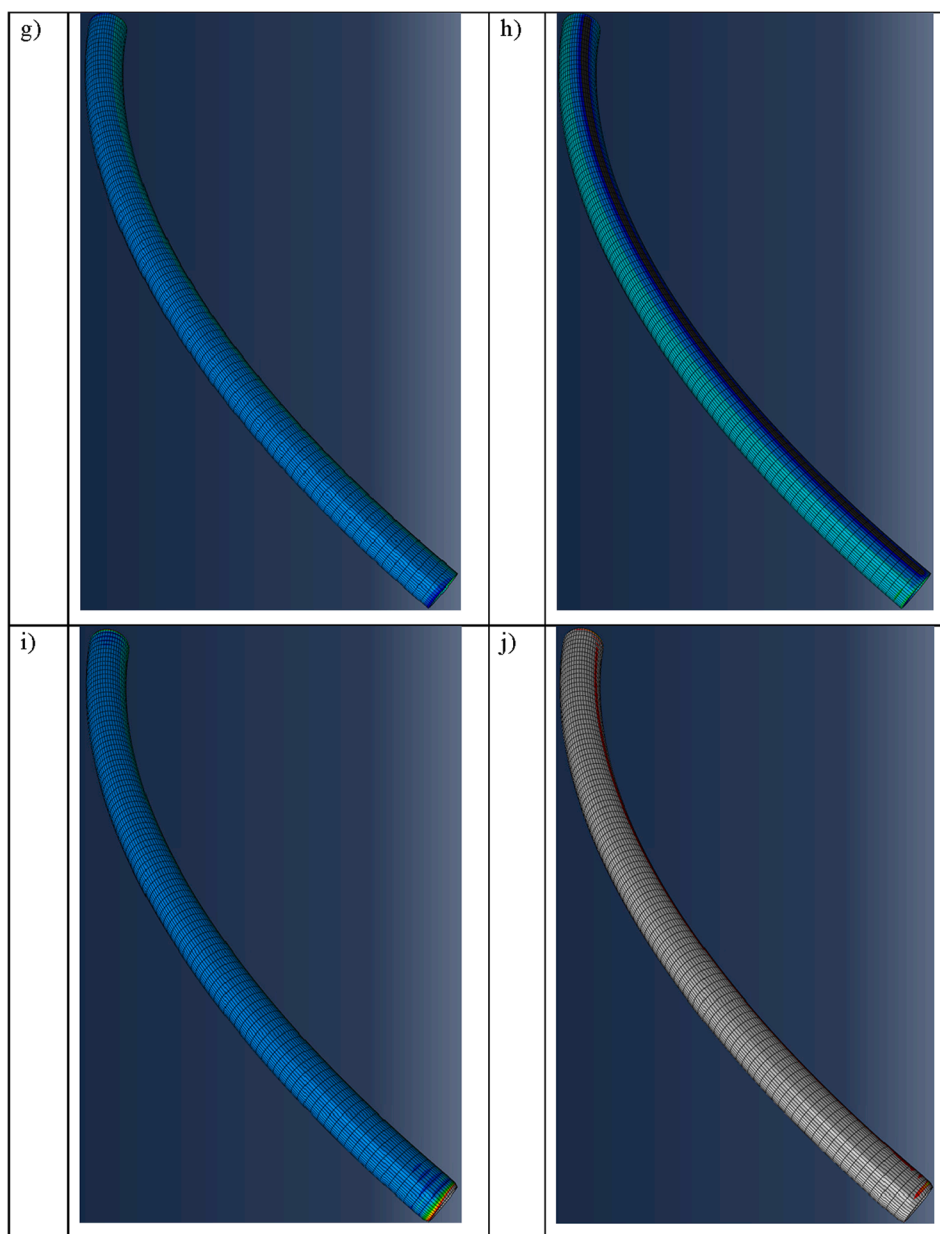

Fig. 8. Contour plots of the hydrostatic pressure and Von Mises equivalent stress of the lead sheathing after bending under different loading conditions and assembly configurations.

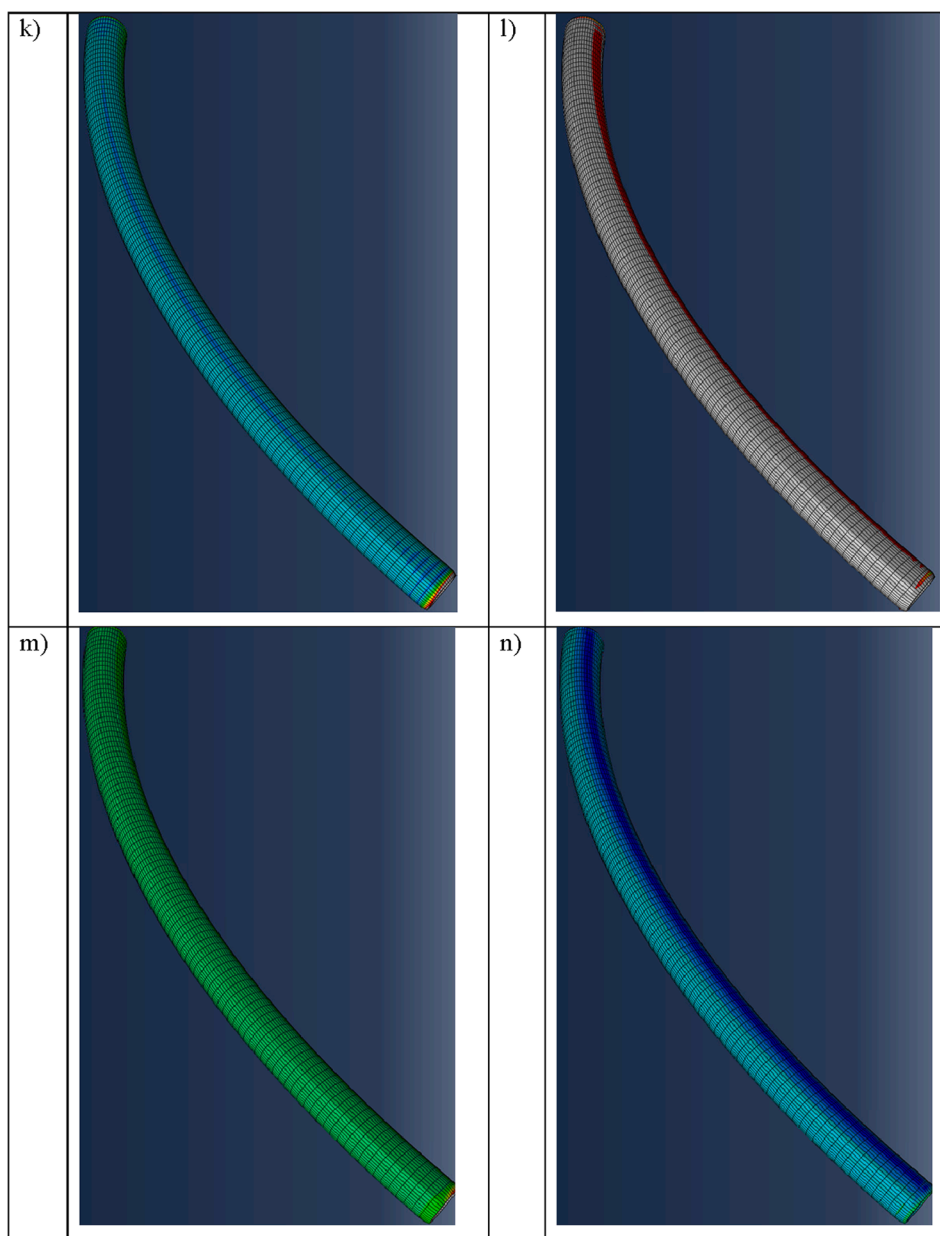**Fig. 8.** (*continued*).
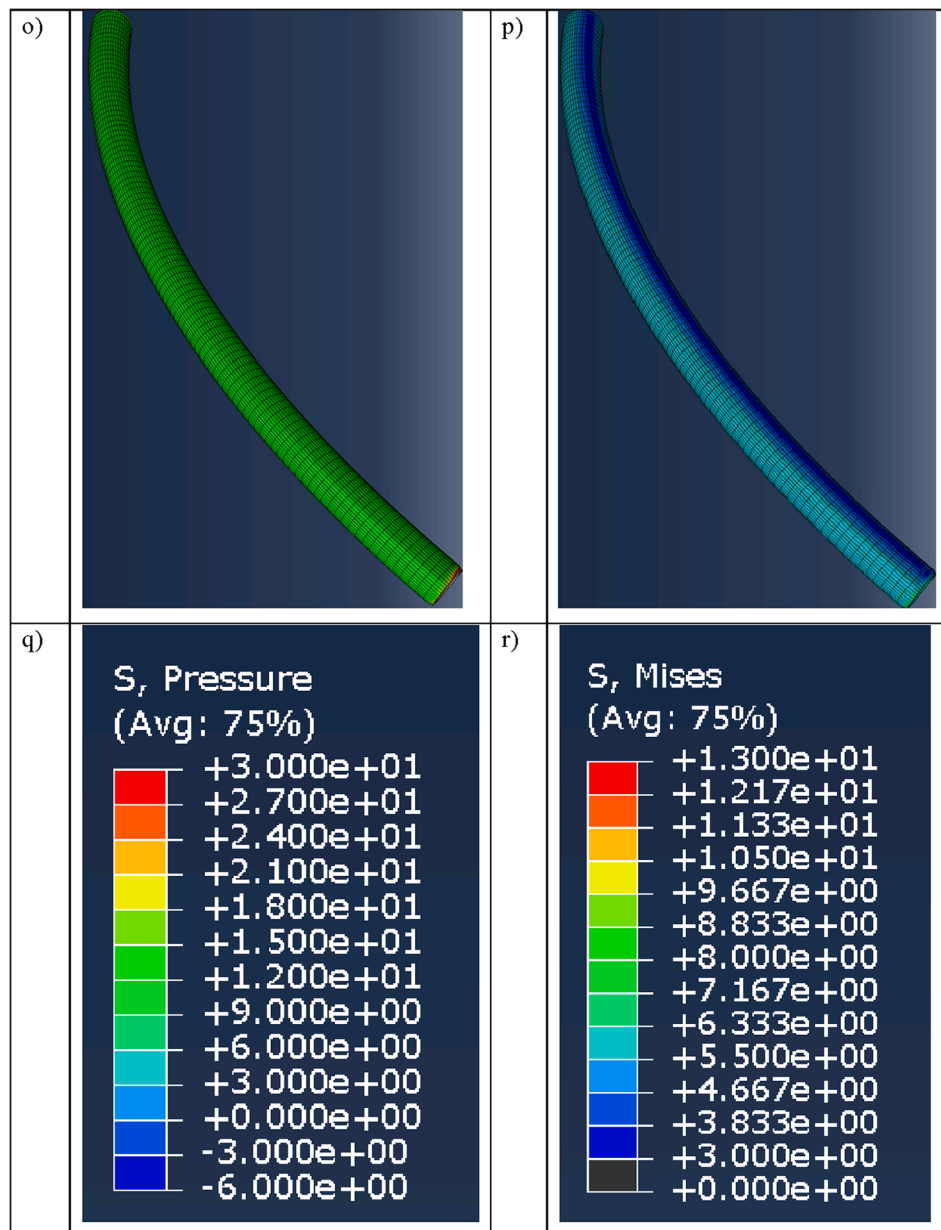
Fig. 8. (*continued*).

Fig. 8. (*continued*).

Fig. 8. (*continued*).

Table 8
Structural and loading conditions corresponding to the contour plot in Fig. 8.

Figures	Loading configuration	Tape winding angle [°]	Viscous analysis
a, b	Test-like	60	OFF
c, d	Test-like	80	OFF
e, f	Test-like	60	ON
g, h	Test-like	80	ON
i, j	Dynamic application	60	OFF
k, l	Dynamic application	80	OFF
m, n	Dynamic application	60	ON
o, p	Dynamic application	80	ON

References

[1] Moore, Herbert Fisher; Alleman, Norville James. The creep of lead and lead alloys used for cable sheathing, a report of an investigation conducted by the Engineering Experiment Station. University of Illinois, Engineering Experiment Station, Bulletin no. 243. 1932.

[2] Dollins, Curtis Walter; Betzer, Cecil E. Creep, fracture, and bending of lead and lead alloy cable sheathing. University of Illinois, Engineering Experiment Station, Bulletin no. 440. 1956.

[3] Feltham P. On the Mechanism of High-Temperature Creep in Metals with Special Reference to Polycrystalline Lead. Proc Phys Soc London, Sect B 1956;69(12): 1173–88.

[4] David Glyn Havard. Fatigue of lead cable-sheathing alloys. Ontario hydro research quarterly. 1972.

[5] P. Anelli, F. Donazzi, W.G. Lawson. The fatigue life of lead alloy E as a sheathing material for submarine power cables. IEEE Transactions on Power Delivery. Volume: 3, Issue: 1. 1988.

[6] Sahota MK, Riddington JR. Compressive creep properties of lead alloys. Mater Des 2000;21:159–67.

[7] Viespoli, Luigi Mario; Johanson, Audun; Alvaro, Antonio; Nyhus, Bård; Sommacal, Alberto; Berto, Filippo. (2018) Tensile characterization of a lead alloy: creep induced strain rate sensitivity. Materials Science & Engineering: A. vol. 744.

[8] Viespoli, Luigi Mario; Johanson, Audun; Alvaro, Antonio; Nyhus, Bård; Berto, Filippo. (2019) Strain controlled medium cycle fatigue of a notched Pb-Sn-Cd lead alloy. Engineering Failure Analysis. vol. 104.

[9] Johanson, Audun; Viespoli, Luigi Mario; Nyhus, Bård; Alvaro, Antonio; Berto, Filippo. (2018) Experimental and numerical investigation of strain distribution of notched lead fatigue test specimen. MATEC Web of Conferences. vol. 165:05003.

[10] Viespoli, Luigi Mario; Johanson, Audun; Alvaro, Antonio; Nyhus, Bård; Berto, Filippo. (2019) Room temperature creep mechanism of a Pb-Sn-Sb lead alloy. Procedia Structural Integrity. vol. 18.

[11] Johanson, Audun; Viespoli, Luigi Mario; Alvaro, Antonio; Berto, Filippo. (2019) Small and Full-Scale Fatigue Testing of Lead Cable Sheathing. ISOPE - International Offshore and Polar Engineering Conference. Proceedings.

[12] Huang ZY, Pilgrim JA, Lewin PL, Swingler SG, Payne D. Current rating methodology for mass impregnated HVDC cables. Electrical Insulation Conference (EIC) 2013.

[13] Huang ZY, Pilgrim JA, Lewin PL, Swingler SG, Tzemis G. Numerical thermo-mechanical stress analysis for HVDC Cables. Electrical Insulation Conference 2014.

[14] Manson SS, Halford GR. 'Fatigue and Durability of Metals at High Temperatures', ASM. International 2009.

[15] Bonacuse Peter. Elevated Temperature Axial and Torsional Fatigue Behavior of Haynes 188. J Eng Mater Technol 1995.

[16] Ildstad E. Rolf Hegerberg 'Cavity Formation in Mass-Impregnated HVDC Subsea Cables-Mechanisms and Critical Parameters'. IEEE Electr Insul Mag 2014.